Research Article

Optimizing Methyl Orange Degradation via Electro-Fenton with Copper Foam Cathode: A Comparative Approach Using Iron Waste vs. Iron Salts and Exploring Catalyst and Cathode Durability

Zahraa Majeed Hameed and Rasha Habeeb Salman*
Department of Chemical Engineering, College of Engineering, University of Baghdad, Baghdad, Iraq

* Corresponding author. E-mail: rasha.habeeb@coeng.uobaghdad.edu.iq DOI: 10.14416/j.asep.2025.05.002
Received: 29 October 2024; Revised: 8 January 2025; Accepted: 18 February 2025; Published online: 7 May 2025

Abstract
The use of foam electrodes as a cathode has proven its efficiency in wastewater treatment. In this study, methyl orange (MO) was treated by Electro-Fenton technology (EFT) using a copper foam (Cf) as a cathode. EFT was an advanced strategy for MO degradation, which accomplished excellent degradation efficiency (%Re_{MO}) exceeded 98% over 35 min treatment period at prime conditions using 0.124 mM of iron salts ($FeSO_4.7H_2O$), 0.3 LPM of air flow, 0.2 mA/cm^2 of current density (CD), and initial pH of 3.0. The outcomes showed that the air flow rate had the main impact on the %Re_{MO}. Furthermore, the contribution of anodic oxidation (AO) to dye removal was investigated to distinguish its role relative to the EFT mechanism, revealing that the MO degradation was government by EFT. Additionally, iron waste (IW) demonstrated high efficacy as a heterogeneous electro-Fenton catalyst, with both the IW and Cf cathode exhibiting excellent reusability and stability. These findings highlight the potential for integrating sustainable materials and processes in dye removal applications, advancing both efficiency and cost-effectiveness.

Keywords: Box-Behnken design, Copper foam, Electro-Fenton, Iron waste, Methyl orange

1 Introduction

The increasing global demand for freshwater is one of the most serious environmental challenges of our time. This demand is driven by rapid population growth, urban expansion, and industrial activities that require significant volumes of water [1]. According to the United Nations (2021), global water demand is projected to rise by 55% by 2050, exacerbating water scarcity and threatening ecosystems and local economies alike. Population growth and urbanization have placed immense stress on freshwater resources. Urban expansion not only directly increases water consumption through residential, agricultural, and industrial needs but also affects natural hydrological systems. For example, impermeable urban surfaces reduce groundwater recharge, while increased wastewater discharge contaminates existing freshwater reserves. Okafor *et al.*, highlight that cities in developing nations often face significant challenges in meeting rising water demands due to limited access to sustainable water resources [2]. Additionally, agriculture accounts for approximately 70% of global freshwater usage, primarily for irrigation. However, inefficient irrigation systems lead to significant water waste [3], [4]. Moreover, certain industries play a disproportionate role in water consumption and contamination for example energy and mining industries, power generation, especially thermal plants, consumes large quantities of water for cooling systems while mining operations contaminate water with heavy metals and other pollutants. Textile and dye industries are other examples of industries that consume large amounts of water, as well as wastewater that is highly contaminated with dyes, metals and organics [5]. Furthermore, the water sources are exposed to pollution due to the discharge of untreated water, the widespread use of pesticides and chemicals in agriculture [6]. Water pollution is a critical problem facing the world because it causes

significant harm to human health, aquatic life and the environment [7], [8].

Dyes are among the most environmentally polluting industrial wastes, they are widely used in many industries such as food, paper, textile, plastics, etc. [9], [10]. It is difficult to classify dyes under a single system due to their vast diversity in sources, chemical structures, and application methods. They vary in their preparation methods; there are natural dyes extracted from minerals, plants, or animals and synthetic dyes produced chemically [11], [12]. Additionally, dyes differ in their chemical structures, including Azo dyes, anthraquinone dyes, and phthalocyanine dyes, among others [13]. Furthermore, based on methods of application, dyes are categorized as acidic (anionic), basic (cationic), mordant, and direct dyes [14]. This wide range of diversity makes it challenging to categorize dyes under a single comprehensive classification system. Dyes pose a threat to the environment and living organisms due to their toxicity, which causes cancerous diseases [15], [16] at lower concentrations. Dyes are still very noticeable and can interfere with photosynthesis by depleting the oxygen that is required by living organisms [17], [18]. Therefore, there is an urgent need to treat water contaminated with dyes [19].

Several reasons made Methyl Orange (MO, an acidic Azo dye) the source of interest in this research, as its structure having –N=N– and aromatic groups that cause great harm to human health and aquatic life due to its high toxicity, solubility in water, and difficulty in biological decomposition [20]. Besides it was widely utilized in many industries and applications such as leather, pH indicator, cosmetic, and textile, thus causing greater amounts of pollutants [21].

Many technologies have been utilized to treat polluted water with dyes, which include liquid membrane [22], filtration [23], adsorption [21], biological process [24], electrocoagulation [25], and advanced oxidation [26]–[28]. Although these processes are efficient in removing dyes, they contain some drawbacks, for example, the physical methods (membrane, filtration, and adsorption) suffer from fouling problems and toxicity of some of the adsorbents used. Moreover, besides the requirement for regeneration and the use of chemicals for desorption processes [29], [30]. Biological technologies limited by certain working conditions, need a longer time for treatment in addition to the fact that most dyes are resistant to biological degradation [31], [32]. Chemical and photodegradation treatments lead to the generation of secondary pollutants and often involve the use of costly catalysts [33], [10]. Therefore, it was necessary to find a simple and effective way to remove dyes, in addition to working on improving them to become inexpensive and environmentally friendly.

Electro-Fenton technology (EFT) is an attractive method that has proven its efficiency in removing and degrading dyes [34], [35]. EFT is one of the electrochemical advanced oxidation technologies (EAOTs) that is based on the combination of Fenton's principles with electrochemical oxidation and formation of a non-selective and strong oxidation agent [hydroxyl radical ($OH^{\bullet}$)] as shown in Equation (1) [36]. EFT was distinguished from the traditional Fenton by generating hydrogen peroxide (H_2O_2) electrolytically using a suitable cathode to catalyze the reduction reaction of the two electrons with oxygen (O_2) (Equation (2)). EFT is superior to the Fenton method in several points: 1) continuous electrical generation of H_2O_2, which leads to improved control of oxidation reactions [37], 2) reducing the costs and risks of transporting and storing H_2O_2 as well as maintaining its effectiveness by decreasing the possibility of its immediate decomposition [35], and 3) continuous regeneration of Fenton catalyst (Fe^{2+}) by reduction of ferric ions (Fe^{3+}) on the cathode surface (Equation (3)), which significantly reducing iron sludge production while decreasing the amount of (Fe^{2+}) required for reaction [38].

$$H_2O_2 + Fe^{2+} \rightarrow OH^{\bullet} + OH^{-} + Fe^{3+} \quad (1)$$

$$O_2 + 2H^{+} + 2e^{-} \rightarrow H_2O_2 \quad (2)$$

$$Fe^{3+} + e^{-} \rightarrow Fe^{2+} \quad (3)$$

Another path that O_2 molecules can take is through their reduction reaction with 4-electrons, which reduces the electrochemically generated H_2O_2 and decreases the removal efficiency. Therefore, choosing appropriate cathodes that promote the H_2O_2 formation is a critical issue, as illustrated in Equation (4) [39]. Three-dimensional (3D) electrodes have attracted the attention of many researchers because they are characterized by their porous structure, which improves the rate of O_2 mass transfer and enhances the electrochemical processes by increasing the affectivity of using space and time. In other words, they can treat larger quantities of pollutants or produce more products for the same space and time compared to 2D

electrodes [19], [40]. To achieve maximum benefit, metal foam electrodes were employed, which are known for their high conductivity in addition to the previously mentioned features [41]. Nickle foam (Nf) [42], Copper foam (Cf) [39], and Iron foam [43] are examples of metal foam service as efficient electrodes in EFT. Goujun *et al*., [44] studied the employing of Cf as a cathode in EFT and they found that Cf promoted the generation of H_2O_2 (Equation (2)) as well as the reduction reaction of Fe^{3+} (Equation (3)). Also, Qian *et al*., [45] made a comparison between the performance of Cf and Nf for the removal of p-nitrophenol by EFT. They concluded that Cf improved $OH^{\bullet}$ production better than Nf. These reasons were enough to choose Cf as a working electrode.

$$O_2 + 4H^+ + 4e^- \rightarrow 2H_2O \quad (4)$$

Several characteristics must be possessed in the electrodes, which are utilized as anodes, including good conductivity and high stability in physical and chemical terms, in addition to their resistance to deterioration and corrosion, which leads to the possibility of repeated use, and economic cost. The most important characteristic is that they have a high potential for O_2 evaluation (non-active anodes) [46]. Although Boron-Doped-Diamond (BDD) was known for its high O_2 overpotential that made it an effective anode in EAOTs, its high cost limited its widespread use [47]. In contrast, carbon electrodes have proven their effectiveness as anodes, beside they are cheap, available, non-toxic, and have high porosity with enough surface area for improving the mass transfer of treated solution [38]. Therefore, Porous Graphite (PG) was employed as an anode.

According to the physical nature of the EFT catalysts, this technology was classified as: 1) homogenous EFT in which the catalyst is soluble in solution (i.e. iron salts), and 2) heterogeneous EFT where the catalyst is in solid form and insoluble (i.e. iron particles, pyrite, iron-loaded zeolite, etc.) [48] [49]. Heterogeneous EFT has attracted significant attention because it is characterized by high catalytic ability and also it facilitates efficient separation and enhances the potential for iron recycling, which is a key factor in maintaining the sustainability of the process operation [50]. Iron waste resulting from industries poses a major environmental threat, where large quantities of iron waste are produced annually. For example, iron casting is one of the largest sources of iron scrape production globally, as studies indicate that for every ton of product, production of one ton of iron scrape and much of this waste is ultimately discarded in landfills, exacerbating environmental problems and squandering valuable resources that could otherwise be reused [51]. In order to minimize environmental damage, advancements in recycling processes are being emphasized, aiming to reduce the need for primary materials and improve the reuse of iron scrap [52]. Therefore, part of this research aims to study the ability to use iron waste (IW) as a cheap alternative source to provide iron ions as IW corrosion under acidic conditions in the effluent, along with the presence of H_2O_2, generates Fe^{2+} (Equation (5)) [53]. Utilizing IW not only mitigates environmental harm but also presents a sustainable solution. Repurposing IW as a Fenton catalyst can pave the way for both eco-conscious practices and significant cost reduction.

$$Fe^0 + 2H^+ \rightarrow Fe^{2+} + H_2 \quad (5)$$

In this work, MO degradation was used as a case study to evaluate the efficiency of homogenous electro-Fenton by utilizing Cu foam as cathode and the impact of operating factors such as current density, air flow rate, and iron salt concentration (Fenton catalyst) was investigated. The response surface methodology (RSM) was utilized to acquire the experimental design, and the results were analyzed to attain the optimum conditions. Moreover, the stability and reusability of the cathode (Cf) were examined and secondly, dependent on the optimal parameters, the possibility of using IW as an alternative to the soluble form of iron salts as a heterogeneous Fenton catalyst and its reusability as well as iron leaching would be studied.

2 Materials and Methods

2.1 *Chemicals*

All chemicals used in this work were of analytical grade without the need for additional purification, as well as deionized water was used to prepare aqueous solutions at ambient temperature. Dimethylamino-azobenzenesulfonate [Methyl Orange (MO)] was obtained from BDH Company and its features with the molecular structure were shown in Table 1. For adjusting the pH of the electrolysis solution, 0.1 M of H_2SO_4 (Sigma-Aldrich) or NaOH (ORPITAL) was used. As an electrolyte, 0.02 M of Na_2SO_4 (SDFCL) was utilized and a certain amount of $FeSO_4.7H_2O$

(CDH, India) and served as a source of Fe^{2+}. The iron scraps utilized in heterogeneous EFT were sourced from a nearby marketplace.

Table 1: The attributes of methyl orange Azo dye.

Synonyms Helianthine, Gold orange, Orange III		**Molecular Structure**
Chemical formula	$C_{15}H_{15}N_3O_2$	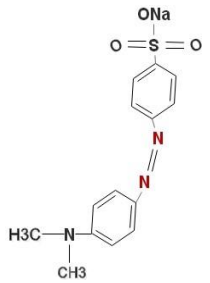
Molar mass	327.34 g/mol	
Melting point	179–182 °C	
λ_{max}	464 nm	
Type	Anionic	

2.2 *System design and apparatus*

All experiments were carried out in an undivided glass batch reactor with 1 L capacity and equipped with 700 ml of 100 mg/L of MO solution. The solution was stirred by using a magnetic stirrer at a speed of 250 rpm. The cell is equipped with a Perspex cover of 10 mm thickness, containing two slots for installing the electrodes and three openings for inserting the thermometer, air distributor, and sampling. Copper foam [(Cf), Xiamen Top New Energy Technology, China] with bulk density and porosity of 0.1–1.5 g/cm³ and ≥ 98%, repressively and dimensions of 130×50×10 mm³ was used as the working electrode, and porous graphite (PG) with dimensions of 130×50×5 mm³ served as an anode, with an active surface area of 32.5 cm². The gap between Cf and PG was 3 cm. To clean Cf, acetic acid (10%) was utilized and then rinsed with deionized water. Before starting any run, an air pump (55 W) was used and contacted to a glass tube with a distributor, through which the electrical cell was supplied with air at a certain flow rate for 20 min, and the air continued to be pumped until the end of the time specified for the experiment (35 minutes). A power supply (0–30 V, 0–5 A) was utilized to equip the cell with a certain current density. In the case of heterogeneous EFT (using iron waste as a catalyst), one cubic piece of iron waste with size of 5×5×5 mm³ and mass of 1 g ± 0.9×10⁻³ was utilized. In the beginning, the iron particle was cleaned by using 0.5 M of H_2SO_4 to remove any oxidation layers and then rinsed with distilled water [54]. Figure 1 illustrates the EFT setup. The cell electrolyte solution consisted of 0.02 M Na_2SO_4 and used $FeSO_4.7H_2O$ as a source of Fe^{2+} ions (in the case of homogenous EFT). All the runs were carried out at room temperature with a fixed initial value of pH = 3.

There were numerous reasons for choosing 3 as the optimum value for pH in this study. First, a value greater than 3 would cause the formation of iron precipitations in the form of Fe^{3+} and promote the consumption of H_2O_2 by OH^-(Equation (6)) [55]. On the other hand, the case of lower pH led to stimulation of the reaction of H_2 evaluation on the cathode surface (Equation (7)). Thus, the proton (H^+) that is needed for generating H_2O_2 would be consumed, in addition to catalyzing its decomposition reaction (Equation (8)) [56]. H_2O_2 can also be depleted by its reaction with H^+ to form $H_3O_2^+$ (Equation (9)) [34]. Finally, the too acidic solution led to the exhaustion of the Fenton catalyst (Fe^{2+}) in the form of $(Fe(H_2O)_6)^{2+}$ [56].

$$H_2O_2 + 2OH^- \rightarrow O_2 + 2H_2O + 2e^- \quad (6)$$

$$2H^+ + 2e^- \rightarrow H_2 \quad (7)$$

$$H_2O_2 + 2H^+ + 2e^- \rightarrow 2H_2O \quad (8)$$

$$H_2O_2 + H^+ \rightarrow H_3O_2^+ \quad (9)$$

The degradation efficiency of methyl orange ($\%Re_{MO}$) was determined by using UV-9200 spectrometers (UK) at 464 nm by applying Equation (10) [35].

$$\%Re_{MO} = \frac{C_0 - C_{35}}{C_0} \text{x}100 \quad (10)$$

Where, C_0 and C_{35} are the concentration of MO (mg/L) at the starting and the ending time of the experiment (35 min), respectively. Besides color detection, the chemical oxygen demand (COD) detection would be measured with the Lovibond Water Testing reactor to approve organic removal. Therefore, at optimum conditions, 2 mL of treated solution was mixed with an oxidizing agent ($K_2Cr_2O_7$) and oxidized within 2 h at 150 °C. The COD value for initial and final samples would be measured with Photometer-System MD200.

The energy consumed during the treatment process (EC, kWh/kg MO) was determined by using Equation (11) [19].

$$EC = (E_{cell} \times t \times I \times 1000)/[(C_0 - C_{35}) \times V_s] \quad (11)$$

Where, E_{cell} is the cell voltage in *V*, *t* is time in *h*, *I* is applied current in *A*, C_0-C_{35} is the decay in MO

concentration and V_s is the treated volume of the solution in L.

To ensure the accuracy of the results and minimize potential errors, each experiment was replicated at least twice.

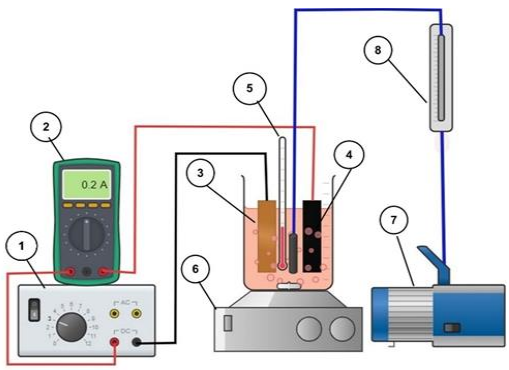

Figure 1: The setup of the Electro-Fenton process: (1) power supply, (2) multimeter, (3) copper foam electrode, (4) porous graphite electrode, (5) thermometer, (6) magnetic stirrer, (7) air pump, (8) air flow meter.

2.3 *Characterization of electrodes*

The surface of the cathode (Cf) and the anode (PG) was examined by utilizing a scanning electron microscope (FEI-company) and the SEM images of these electrodes before reaction are shown in Figures 2 and 3. It was clear from Figure 2 that Cf exhibited a three-dimensional network structure characterized by a regular distribution of multiple interconnected pores and its colorful SEM photos displayed the elements of the foam (Cu and C), while PG demonstrated a high level of porosity, with large pores formed among the interconnected structures as shown in Figure 3. The Energy Dispersive X-ray spectroscopy (EDX) from Bruker Company which operated at 100A, 25 kV and XFlash-6110 was employed to identify and detect the composition of electrode elements as illustrated in Figure 4. EDX results showed that Cf and PG consisted of copper and carbon respectively, with trace impurities. For analyzing the crystal structure of three-dimensional material (Cf and GP), an X-ray diffractometer (XRD, Shimadzu) was employed which operated at 40 kV and 30 mA using CuKα radiation. XRD results are shown in Figure 5, which revealed that Cf exhibited a face-centered cube structure and three strong curving peaks at 43.5°, 50.6°, and 74.3°, which corresponded to the crystal planes of copper structure (111), (200), and (220) in accordance with JCPDS card No. 04-0836 [57]. Whereas the XRD pattern for PG showed a strong diffraction peak at $2\theta = 26.382°$ according to the graphite crystal plane (002) [40].

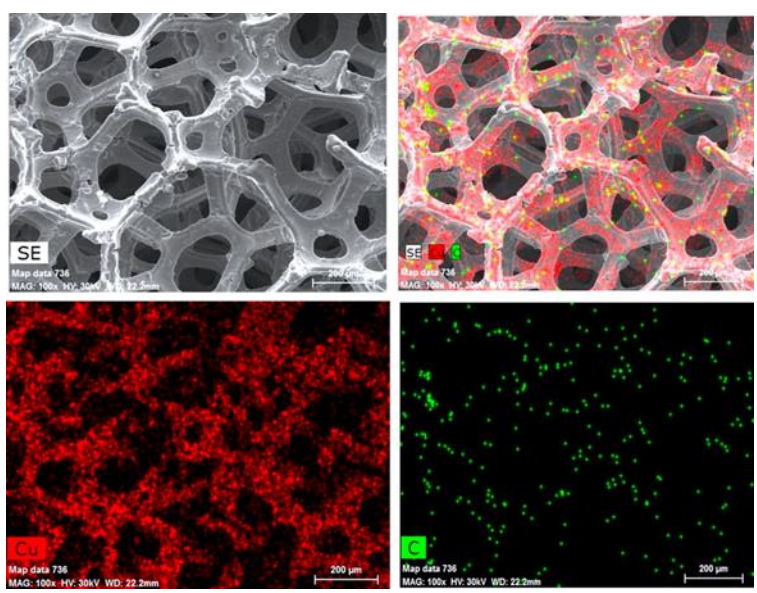

Figure 2: Colorful SEM photo of Cf (with a magnification of 200µm) before reaction.

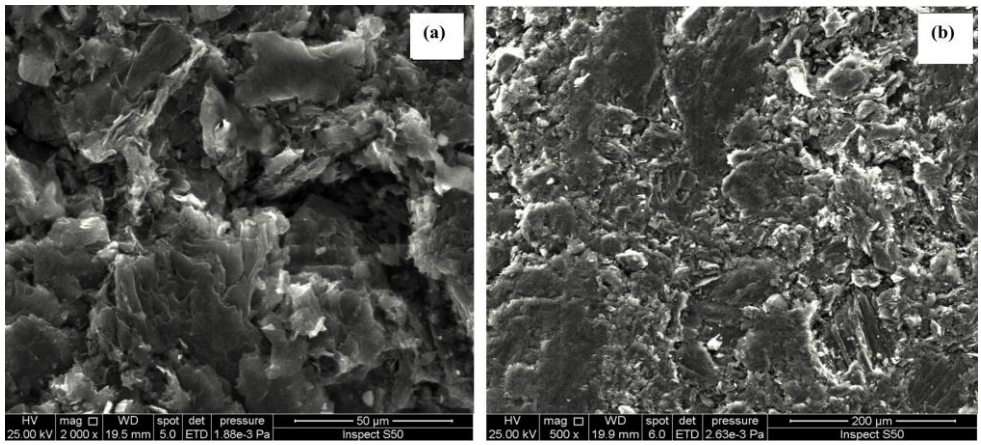

Figure 3: SEM for PG before reaction (a) at magnification of 50 µm, and (b) at magnification of 200 µm.

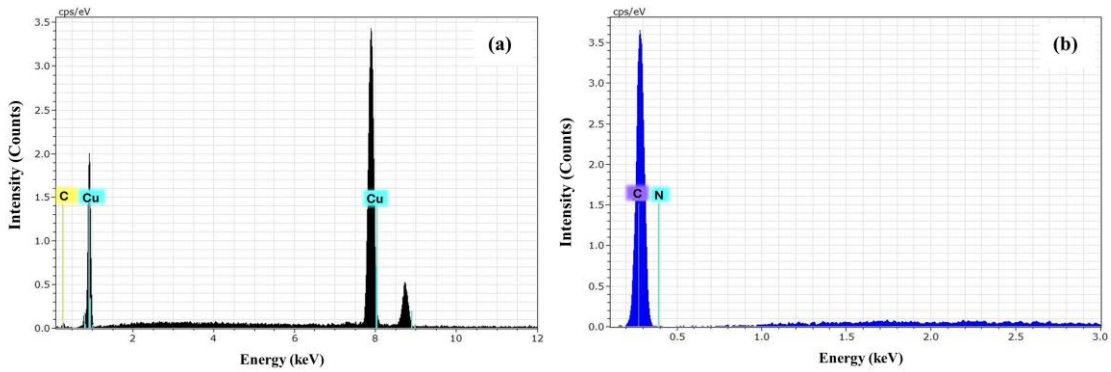

Figure 4: EDX results of (a) Cf, and (b) PG.

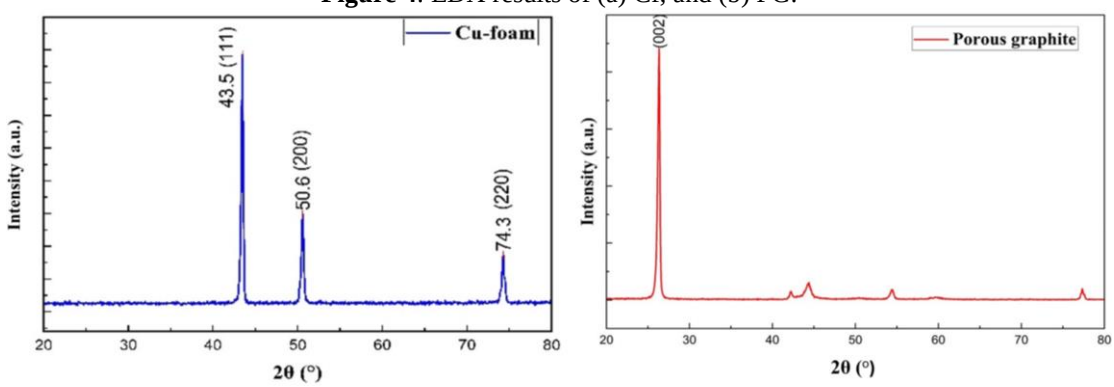

Figure 5: XRD results for Cf and PG.

2.4 *Experimental design*

To identify the optimal conditions for achieving the highest $\%Re_{MO}$ with the fewest number of experiments, Response Surface Methodology (RSM) was used. In this study, the Box-Behnken (BB) design was the most effective approach to describe the optimization process because it was well-structured and financially efficient [58]. The impact of three process variables (current density (CD), iron ion concentration [Fe^{2+}], and air flow) at three different levels (–1, 0, and +1) was taken into account. The coded variables with their levels are illustrated in Table 2. Table 3 demonstrates the layout of BB experimental design, and the experimental data were analyzed with Minitab 19 software. The model is outlined in Equation (12) characterizing the mathematical relationship between the independent factors and the response utilizing the least-squares approach [35].

$$F(x) = \beta_0 + \sum \beta_i x_i + \sum \beta_{i_i} x_i^2 + \sum \beta_{i_j} x_i x_j \quad (12)$$

Where, $F(x)$ is the removal efficiency of MO (the response), β_0 is constant, β_i, β_{i_i}, and β_{i_j} are the regression coefficients, x_i and x_j are independent factors.

Table 2: The coded process parameters and their ranges.

Variables and their Symbols	Variables Ranges		
	-1	0	+1
A, CD (mA/cm^2)	3	5.5	8
B, air flow (LPM)	0.1	0.2	0.3
C, [Fe^{2+}] (mM)	0.1	0.2	0.3

Table 3: The experimental array of BB design for MO removal.

Run	Bk.	Coded Value			Actual Value		
		A	B	C	CD (mA/cm^2), A	Air flow (LPM), B	[Fe^{2+}] (mM), C
1	1	0	-1	-1	5.5	0.1	0.1
2	1	-1	0	1	3.0	0.2	0.3
3	1	-1	0	-1	3.0	0.2	0.1
4	1	0	-1	1	5.5	0.1	0.3
5	1	1	1	0	8.0	0.3	0.2
6	1	0	0	0	5.5	0.2	0.2
7	1	1	0	-1	8.0	0.2	0.1
8	1	0	1	-1	5.5	0.3	0.1
9	1	0	0	0	5.5	0.2	0.2
10	1	1	-1	0	8.0	0.1	0.2
11	1	-1	-1	0	3.0	0.1	0.2
12	1	0	1	1	5.5	0.3	0.3
13	1	0	0	0	5.5	0.2	0.2
14	1	1	0	1	8.0	0.2	0.3
15	1	-1	1	0	3.0	0.3	0.2

3 Results and Discussion

3.1 *Formulation of a regression model and implementation of comprehensive statistical analysis*

According to RSM coupling with BB model via Minitab-19, the impact of three EFT parameters for MO removal including CD (A), air flow (B), and [Fe^{2+}] (C) were examined and analyzed. Table 4 demonstrates the experimental results that can be well characterized by a quadratic model, which is illustrated in Equation (13).

$$\%Re_{MO} = 72.37 + 4.440\,A + 83.0\,B + 24.7\,C - 0.3996\,A^2 - 68.7\,B^2 - 160.1\,C^2 - 3.61\,A\,B + 6.48\,A\,C - 63.1\,B\,C \quad (13)$$

As seen in Table 4, the ranges of $\%Re_{MO}$ and EC were (88.5062 to 99.3988 %) and (3.6515 to 21.0460 kWh/kg MO), respectively. Analysis of variance (ANOVA) is known as a very efficient statistical way of testing the response of the process by determining whether the variables significantly impact the response and identifying, which variables or interactions between variables have the most effect [58]. The results of the model's ANOVA are presented in Table 5. The most important statistical elements in the ANOVA table were *P*-value and F-value because they determine the extent to which the model and its parameters are statistically significant. An F-value greater than 4 with a *P*-value less than 0.05 suggests that there is a significant impact of factors on the response, and the observed results are unlikely to be due to random variation [19]. Therefore, as evident from Table 5, the model was significant as the *P*-value was 0.001 and the F-value was 33.36 with model contribution% of 98.36%. The *P*-value of lack of fit was 0.096 (*P*-value > 0.05), which means insignificant, this indicates that the model is capable of accurately predicting the response levels [59]. The

air flow had the highest impact on the response ($\%Re_{MO}$) as its contribution% was 32.32% followed by [Fe^{2+}] (16.18%) and CD (14.63%).

3.2 *The impact of working factors on MO degradation*

Based on RSM and for more investigation, Figures 6–8 illustrate contour with 3D surface, and 2D plots, correspondingly to study the impact and the interaction of each process parameter on the $\%Re_{MO}$. Figure 6 illustrates the effect of CD (3 to 8 mA/cm^2) on MO removal over a range of air flow (0.1 to 0.3 LPM) at a fixed [Fe^{2+}] of 0.2 mM. As observed from the contour graph in Figure 6(a), the MO reduction efficiency > 98% can be potentially achieved at a region where air flow varies in a range of 0.2 LPM to 0.3 LPM over a range of CD (4 to 7.5 mA/cm^2). The elimination efficiency increased with the increase of the air flow as displayed in Figure 6(b), which means that air flow had a significant effect on the response. This can be seen by comparing the experiments 1 and 8 in Table 4, where at 5.5 mA/cm^2 of CD with 0.1 mM of [Fe^{2+}]. The removal efficiency improved from 93.8365% to 99.3988% when the air flow rose from 0.1 LPM to 0.3 LPM. This improvement came from the fact that increasing air flow led to an increase in the amount of dissolved oxygen, which is necessary for the electrosynthesis of H_2O_2 (Equation (2)) through the reduction reaction and thus increased the amount of oxidizing agent ($OH^{\bullet}$) as mentioned in Equation (1), which in turn improved the removal rate. In addition, increasing the flow of air enhanced the mass transfer rate within the electrical cell [59]. Figure 6(c) clearly shows the positive effect of increasing CD on $\%Re_{MO}$ to a certain extent, after which any increase in CD led to an adverse impact on the elimination efficiency. This outcome can be attributed to the principle that a higher CD elevates the potential of cathode, thereby intensifying oxygen reduction at the surface of cathode. Moreover, increasing CD improved the regeneration of Fe^{2+} from Fe^{3+} reduction (Equation (3)) [60]. On the other hand, at a higher value of CD (excessed the optimum), the removal rate declined for all levels of air flow because, at high CD, side reactions promoted such as H_2 evolution at the cathode (Equation (7)), O_2 discharge at the anode, and $OH^{\bullet}$ side reaction, which is illustrated in Equations (14) and (15), respectively [56]. In addition, the high CD caused an increase in the EC as can be seen in the results of Table 4. Therefore, the adjustment of CD not only enhanced the removal efficiency but also reduced the operating cost as CD is the critical factor that affected EC [35].

$$2H_2O \rightarrow 4H^+ + O_2 + 4e^- \quad (14)$$

$$2\,OH^{\bullet} \rightarrow O_2 + 2H^+ + 2e^- \quad (15)$$

Table 4: The results of $\%Re_{MO}$ and EC.

Run	Bk.	A, CD (mA/cm^2)	B, air flow (LPM)	C, [Fe^{2+}] (mM)	$\%Re_{MO}$		E (volt)	EC (kWh/kg MO)
					Real	Predicted		
1	1	5.5	0.1	0.1	93.8365	94.140	4.7	10.2868
2	1	3.0	0.2	0.3	88.5062	88.833	3.2	4.6649
3	1	3.0	0.2	0.1	95.9273	95.337	3.3	3.6515
4	1	5.5	0.1	0.3	92.7545	92.141	4.9	11.2564
5	1	8.0	0.3	0.2	97.7898	97.503	6.3	18.9371
6	1	5.5	0.2	0.2	97.9089	97.734	4.9	9.201
7	1	8.0	0.2	0.1	95.5229	95.196	5.8	17.7318
8	1	5.5	0.3	0.1	99.3988	100.013	4.8	8.7447
9	1	5.5	0.2	0.2	97.4298	97.734	4.9	9.252
10	1	8.0	0.1	0.2	94.6731	94.696	5.5	21.0460
11	1	3.0	0.1	0.2	89.5038	89.791	3.4	4.2019
12	1	5.5	0.3	0.3	95.7923	95.489	4.6	10.7194
13	1	5.5	0.2	0.2	97.8623	97.734	4.9	9.207
14	1	8.0	0.2	0.3	94.5861	95.177	5.8	18.4413
15	1	3.0	0.3	0.2	96.2286	96.205	3.1	3.9981

Table 5: The results of ANOVA for MO removal.

Source	DF	Seq. SS	Contr.	Adj. SS	Adj. MS	F-Value	*P*-value
Model	9	129.365	98.36%	129.365	14.3739	33.36	0.001
Linear	3	83.026	63.13%	83.026	27.6754	64.23	0.000
A	1	19.239	14.63%	19.239	19.2386	44.65	0.001
B	1	42.512	32.32%	42.512	42.5116	98.66	0.000
C	1	21.276	16.18%	21.276	21.2761	49.38	0.001
Square	3	30.980	23.56%	30.980	10.3265	23.97	0.002
AA	1	20.336	15.46%	23.028	23.0284	53.44	0.001
BB	1	1.183	0.90%	1.745	1.7450	4.05	0.100
CC	1	9.460	7.19%	9.460	9.4602	21.96	0.005
2-WayInteraction	3	15.359	11.68%	15.359	5.1198	11.88	0.010
AB	1	3.255	2.47%	3.255	3.2546	7.55	0.040
AC	1	10.512	7.99%	10.512	10.5115	24.40	0.004
BC	1	1.593	1.21%	1.593	1.5933	3.70	0.113
Error	5	2.154	1.64%	2.154	0.4309	-	-
Lack-of-Fit	3	2.015	1.53%	2.015	0.6716	9.62	0.096
Pure Error	2	0.140	0.11%	0.140	0.0698	-	-
Total	14	131.520	100.00%	-	-	-	-
Model Summary			S	R^2	R^2(adj.)	Press	R^2(pred.)
			0.65641	98.36%	95.41%	32.5513	75.25%

The interaction effect of [Fe^{2+}] with CD on MO reduction at fixed air flow (0.2 LPM) was investigated as displayed in Figure 7. The peak in the contour graph shown in Figure 7(a), demonstrated that the best removal efficiency was attained within the range found within this circular area. It revealed a distinct interaction between [Fe^{2+}] and CD on%Re_{MO}. From Figure 7(b), the elimination efficiency sharply dropped as [Fe^{2+}] raised and this can be detected from the comparison between runs, 2 and 3 in Table 4 in which at constant CD and air flow at values of 3 mA/cm^2 and 0.2 LPM, respectively, as [Fe^{2+}] dropped from 0.3mM to 0.1 mM, the %Re_{MO} increased from 88.5062% to 95.337%. The excess of [Fe^{2+}] would consume $OH^{\bullet}$ as illustrated in Equation (16) [37] [59]. Figure 7(c) depicted that even at the highest value of CD, the negative effect of increasing [Fe^{2+}] can be observed, but at a slower pace, as shown by the results of experiments 7 and 14, where at a fixed CD (8 mA/cm^2), which is the upper limited value, and at the same constant air flow rate (0.2 LPM), the removal efficiency decreased from 95.5229% to 94.5861% as [Fe^{2+}] rising from 0.1 mM to 0.3 mM [61], [60].

$$Fe^{2+} + OH^{\bullet} \rightarrow Fe^{3+} + OH^{-} \quad (16)$$

At a constant CD (5.5 mA/cm^2), Figure 8 demonstrates the influence of [Fe^{2+}] and air flow on %Re_{MO}. The contour plot (Figure 8(a)) confirmed that MO removal efficiency between 98% and 100% was confined to a specific range where air flow fluctuated between 0.19 LPM and 0.3 LPM, and [Fe^{2+}] levels range from 0.1 to 0.24 mM. Figures 8b-c showed that %Re_{MO} increased with air flow growth with a slight improvement on %Re_{MO} as [Fe^{2+}] increased to 0.15 mM and then %Re_{MO} dropped for any increase beyond this value (0.15 mM). This effect can be observed through the results of runs 1 and 8 from Table 4, where at a fixed value of CD (5.5 mA/cm^2) and [Fe^{2+}] (0.1 mM) the %Re_{MO} enhanced from 93.8365% to 99.3988 with a decrease in EC from 10.2868 to 8.7447 kWh/kg MO when air flow was increased from 0.1 to 0.3 LPM. While, at runs 4 and 12, the improvement in the peak of %Re_{MO} was less (from 92.7545% to 95.7923%) and a decrease in the EC value (decreased from 11.7545 to 10.7194 kWh/kg MO). Although CD value was constant at 5.5 mA/cm^2 and air flow increased from 0.1 to 0.3 LPM, the [Fe^{2+}] was 0.3 mM. The effect of the high value of [Fe^{2+}] on EC was small [35]. As the runs 2 and 11 have the lowest %Re_{MO}values compared to the other experiments, a comparative analysis was done to address the reason behind this difference. In run 2, the higher [Fe^{2+}] (0.3 mM) would increase the availability of iron ions for hydroxyl radical ($OH^{\bullet}$) generation. However, excess Fe^{2+} acts as a scavenger, reacting with $OH^{\bullet}$ to form Fe^{3+}, thereby reducing the oxidative efficiency as shown in Equation (16). This scavenging effect could explain the slightly lower efficiency compared to run 11. While in run 11, a lower [Fe^{2+}] (0.2 mM) minimized scavenging, allowing more $OH^{\bullet}$ to contribute to MO degradation, resulting in slightly better removal efficiency [35]. Therefore, scavenging effects in run 2 due to higher [Fe^{2+}] (0.3 mM) resulted

in $OH^{\bullet}$ scavenging, reducing efficiency despite better aeration. In terms of air flow rate, as seen in run 2, a 0.2 LPM is adequate for oxygen supply, which is essential for H_2O_2 generation at the cathode as illustrated in Equation (2). Whereas in run 11, the reduced air flow rate (0.1 LPM) likely limits H_2O_2 production and reduces $OH^{\bullet}$ generation [62]. Limited aeration in run 11 due to lower air flow rate (0.1 LPM) restricted oxygen availability and slowing H_2O_2 production. However, the reduced $[Fe^{2+}]$ mitigated scavenging, leading to slightly better efficiency. Moreover, both runs operated at a low CD (3 mA/cm^2), which limits the electrochemical generation of H_2O_2 and $OH^{\bullet}$, and reducing efficiency compared to the other experiments [63].

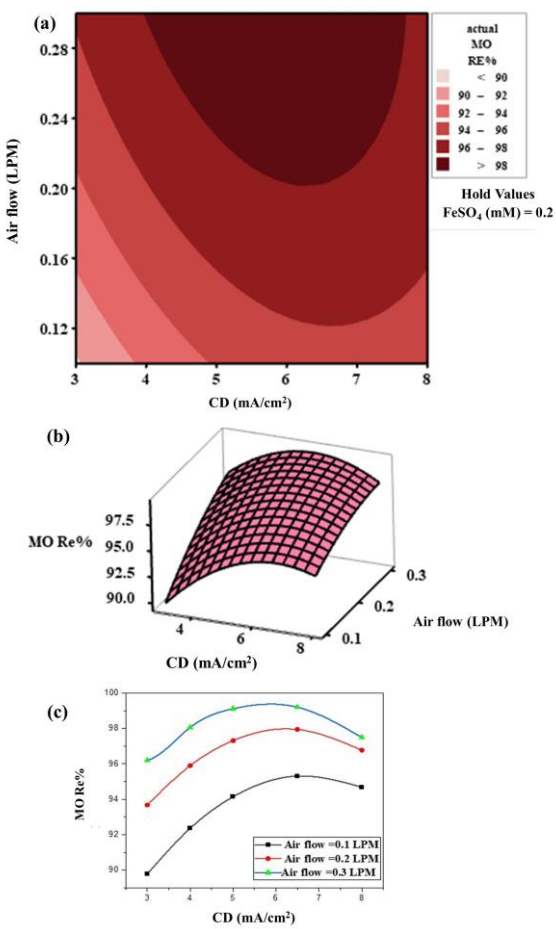

Figure 6: The removal of MO as a function of CD and air flow at $[Fe^{2+}]$= 0.2 mM, (a) contour, (b) 3D surface, and (c) 2D surface plots.

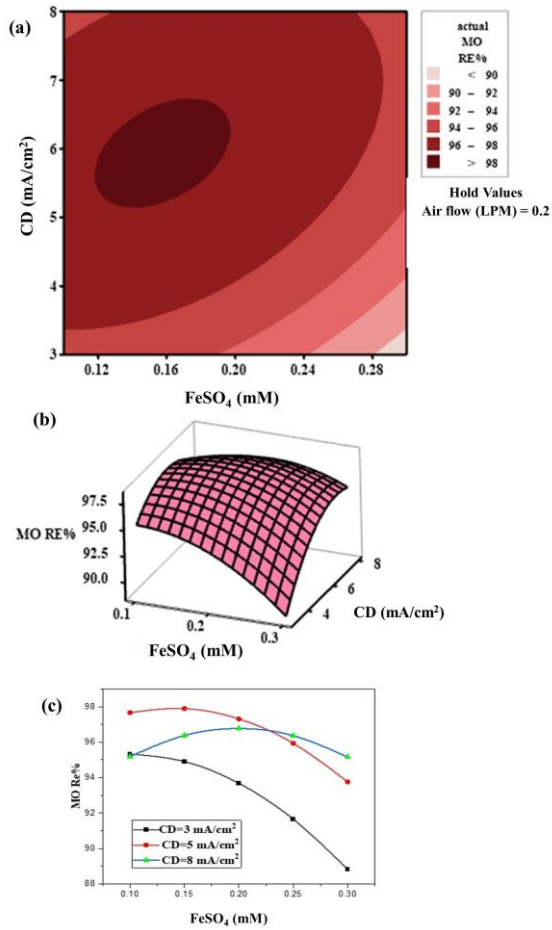

Figure 7: The removal of MO as a function of $[Fe^{2+}]$ and CD at air flow = 0.2 LPM, (a) contour, (b) 3D surface, and (c) 2D surface plots.

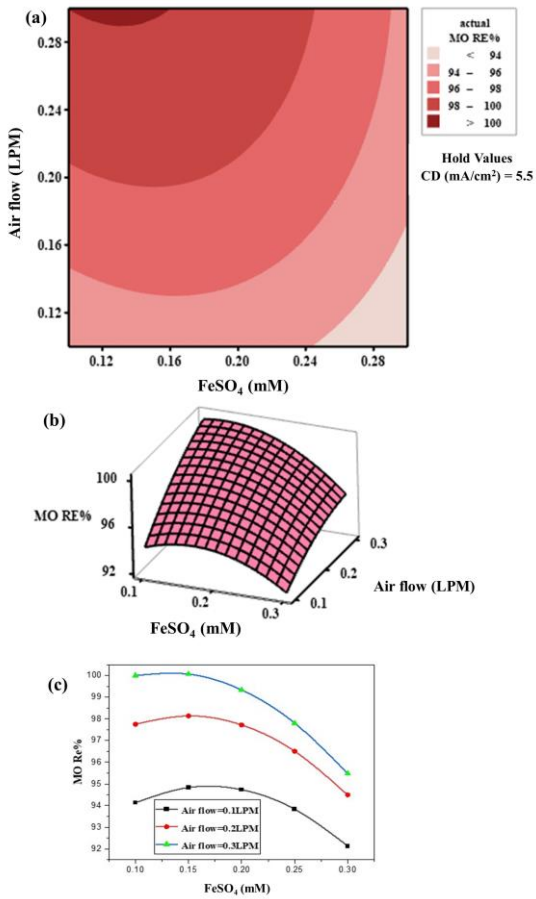

Figure 8: The removal of MO as a function of $[Fe^{2+}]$ and air flow at CD = 5.5 mA/cm^2, (a) contour, (b) 3D surface, and (c) 2D surface plots.

3.3 *The optimization of the EFT and verification of the outcomes*

One of the most important goals of employing BB design for studying and analyzing the results of MO degradation in this work was to find the optimal working conditions to achieve the highest removal with the lowest EC [19]. Table 6 illustrates the optimum value for $\%Re_{MO}$. To validate the performance of BB, a confirmation test was carried out with optimal variables levels as shown in Table 7. The average $\%Re_{MO}$ was 98.86% with EC of 7.87 kWh/kg MO at electrolysis time of 35 min, while earlier study by Adachi *et al*., [63], who used graphite as a cathode in EFT 94.5% removal efficiency of MO was achieved in 60 min with using larger amount of chemicals. This indicates how efficient the Cf electrode was in the degradation of MO. The initial value of COD was 53 mg/L which increased to 154 mg/L within 15 min of electrolysis, and its final value at optimum conditions was 6 mg/L at the end of the experiment.

3.4 *Reusability and stability of cathode electrode (Cf)*

In order to evaluate the reusability of the copper foam (Cf) electrode, consecutive experiments were conducted for the degradation of MO under the optimum conditions (without regeneration treatment). The results showed that the $\%Re_{MO}$ was 97.86% after five successive cycles with a slight decrease from the first run ($\%Re_{MO}$ = 99.03%) as demonstrated in Figure 9 and Table 8. The reasons for this decrease might be due to 1) accumulation of reaction by-products, such as iron hydroxides and organic intermediates which reduces active sites for H_2O_2 generation [64], 2) adsorption of reaction intermediates on the cathode surface which hinders catalytic performance [65], 3) electrochemical reactions lead to gradual erosion of the copper foam thus copper ions (Cu^{2+}) are leached from the cathode under the process conditions, which are secondary pollutants at specific rates [39] because copper ions are toxic to aquatic organisms even at low concentrations. Copper ions can interfere with enzyme systems, disrupt osmoregulation, and accumulate in tissues, leading to bioaccumulation and biomagnification along the food chain. The maximum allowable concentration for Cu^{2+} in drinking water is 1.3 mg/L according to EPA standards [66], [67]**.** Moreover, copper ions might consume H_2O_2 as shown in Equation (17) [44].

$$Cu^{2+} + H_2O_2 \rightarrow Cu^{+} + HO_2^{\bullet} + H^{+} \quad (17)$$

Therefore, the concentration of leached Cu^{2+} was examined after each run. As seen in Figure 9, the $[Cu^{2+}]$ was increased with each cycle until reached final concentration of 0.36 mg/L at the fifth cycle. According to River Maintenance System No. (25) of 1967 of the state of Iraq, the permissible limits for $[Cu^{2+}]$ in wastewater discharged into the water source should not exceed 0.2 mg/L. Therefore, Cf as cathode had good reusability for 3 runs with excellent elimination efficiency and acceptable concentration of Cu^{2+}. The SEM analysis in Figure 10 for Cf before and after 5 runs revealed high stability for Cf cathode which had a similar structure as before reaction concentration of Cu^{2+}. The SEM analysis in Figure 10 for Cf before and after 5 runs revealed high stability for Cf cathode which had a similar structure as before reaction.

Table 6: The optimum conditions for the maximum removal efficiency of MO.

Response	Goal	lower	Target	Upper	Weight	Important
	Max.	88.05	Max.	99.39	1	1
Solution of parameters			Multiple response prediction			
CD, mA/cm^2	Air flow, LPM	[Fe^{2+}], mM	MO% fit	SE fit	95% CI	95% PI
5.22	0.3	0.124	100.18	0.481	(98.944,101.415)	(98.089,102.271)

Table 7: The verification of the optimal result.

Run	CD, mA/cm^2	Air flow, LPM	[Fe^{2+}], mM	E, volt	EC, kWh/kg MO	Actual MO Re%	Average
1	5.22	0.3	0.124	4.7	7.72	99.03	98.86
2	5.22	0.3	0.124	4.7	8.03	98.67	

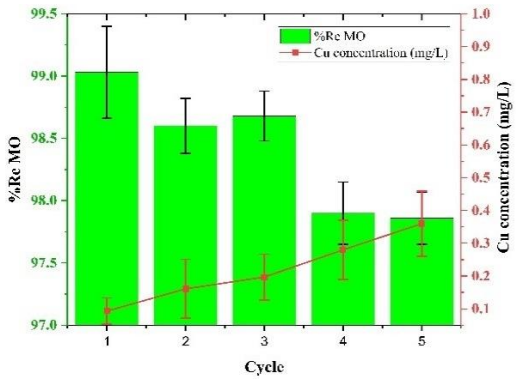

Figure 9: Reusability of Cf cathode and Cu leaching from cathode at the optimum condition for 5 successive runs.

Table 8: The %Re$_{MO}$ over 5 reuse cycles under identical operating conditions.

Cycle	%Re$_{MO}$	Efficiency Loss Relative to Initial Cycle (%)
1	99.03	0
2	98.6	0.43
3	98.68	0.35
4	97.9	1.13
5	97.86	1.17

3.5 *The comparative degradation of MO by anodic oxidation (AO) and EFT*

Since the degradation of pollutants in EFT is achieved by the action of Fenton's reagents combined with AO, which takes place on the anode surface, the elimination of MO was investigated through AO and EFT separately under the optimum conditions without using any source for Fenton catalyst in case of AO. The outcomes displayed in Figure 11 showed that the %Re$_{MO}$ at the end of 35 min was 76.7% by AO while it was 98.6% by EFT. These results are consistent with the findings of Bocos *et. al.*, who established that AO exhibits a constrained capacity for the degradation of dyes [42]. Moreover, EFT was more efficient and achieved higher rates of dye removal due to the continuous generation of highly reactive (OH$^{\bullet}$) in the EFT, which accelerates the degradation of dyes. In contrast, AO primarily releases the generated oxygen species at the anode, which may not be as reactive or effective in breaking down certain complex dye molecules as quickly as the EFT [68], [69]. Therefore, EFT was much more efficient for MO elimination than AO.

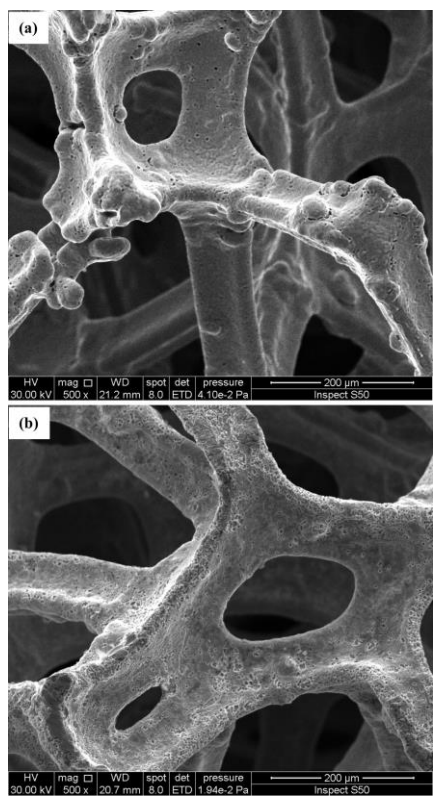

Figure 10: SEM for Cf at a magnification of 200µm (a) before reaction and (b) after 5 successive runs.

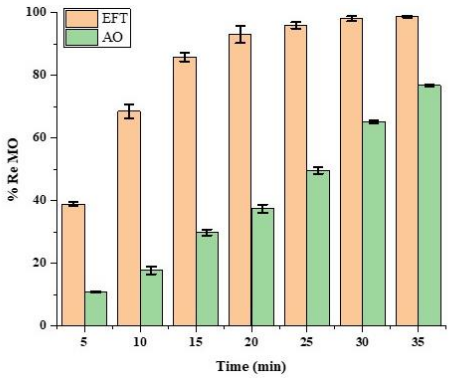

Figure 11: The comparison of EFT and AO for degradation of MO at optimum conditions (CD = 5.22 mA/cm^2, air flow = 0.3 LPM, and [Fe^{2+}] = 0.124 mM).

3.6 *Iron waste (IW) as an alternative source for ferrous ions*

3.6.1 The performance of iron waste

Depending on the optimal conditions, the effectiveness of using iron waste as a cheap source of Fenton catalyst was tested and Table 9 displayed the results of the comparison between the use of $FeSO_4.7H_2O$ (IS) and iron waste (IW) to eliminate MO over time. In the first minutes, it was noted that the removal efficiency using IS was higher than in the case of using IW. The reason for this was that the release of iron ions (Fenton catalyst) from IW was slow at first, but as the electrolysis continued, the removal rate increased and became comparable to or even higher than the removal efficiency with IS due to the release of larger quantities of iron ions [70], [71]. The reusability of the IW catalyst was tested by assessing its ability to remove MO over multiple cycles in the EFT without any regeneration treatments between cycles. This method helps in determining how effectively the catalyst can maintain its performance in degrading contaminations through successive uses without requiring chemical or physical restorations. The results in Figure 12 showed that > 98% of $\%Re_{MO}$ was achieved after four successive runs by utilizing IW. Additionally, the leaching of iron from IW was tracked over the four runs. The results illustrated that as the reaction time increased, the concentration of iron leaching also increased, eventually reaching a final value of 0.872 mg/L at the end of the fourth cycle, which was substantially lower than the discharge limits set by River Maintenance System No. (25) of 1967 of the state of Iraq (iron concentration < 5 mg/L) and the standards of the European Union in which iron concentration is less than 2 mg/L [52].

Table 9: MO degradation by using IS and IW.

Time(min)	$\%Re_{MO}$ with IS	$\%Re_{MO}$ with IW
0	0	0
5	39.19 ± 0.69	38.92 ± 3.51
10	67.33 ± 2.26	64.97 ± 2.73
15	83.76 ± 1.36	82.81 ± 2.62
20	92.01 ± 2.75	91.78 ± 1.77
25	96.01 ± 1.06	96.06 ± 0.39
30	97.88 ± 0.78	97.96 ± 0.19
35	98.68 ± 0.2	98.82 ± 0.23

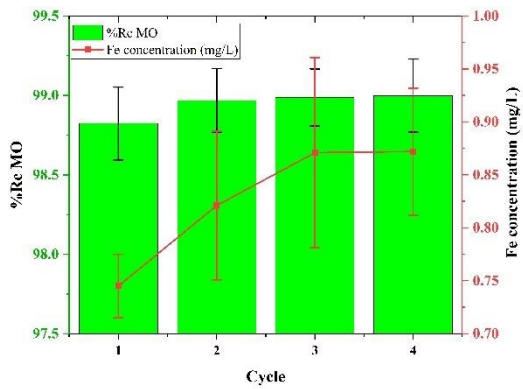

Figure 12: Reusability of IW and Fe leaching from IW at the optimum condition for 4 successive runs.

3.6.2 The characterization of IW

Iron waste, derived from various industrial processes, contains a mixture of iron oxides (Fe^{2+}/Fe^{3+}), metallic iron, and sometimes impurities such as carbon or silicates. As the chemical composition is an important factor that affects its catalytic activity in the electro-Fenton process, EDX analysis was conducted for IW and the results are illustrated in Figure 13(a). The results clearly highlighted iron as the dominant element (Fe= 87.3%), as evidenced by its higher peak appearing in the elemental profile. Iron-rich wastes with minimal impurities (e.g., copper or zinc) typically exhibit higher activity. Rattanachueskul *et al*., showed that para-rubber wood ash, rich in iron oxides, provided high catalytic efficiency due to its chemical composition [72]. Moreover, Scanning Electron Microscopy (SEM) was utilized to provide information about the morphology and microstructural features. In Figure 13(b), the SEM image shows a rough and uneven surface, indicating high surface area, which is beneficial for catalytic reactions as it enhances the dissolution rate of iron ions (Fe^{2+}/Fe^{3+})

into the solution. This ensures a steady supply of reactive iron species for the Fenton reaction. Kazmi *et al*., demonstrated that iron-enriched biochar derived from pistachio shells achieved superior catalytic activity due to increased surface area from reduced particle size [73]. XRD results are shown in Figure 13(c), which revealed that IW exhibited a body-centered cube structure and three strong curving peaks at 43.67°, 65.02°, and 82.34° which corresponded to the crystal planes of iron structure (110), (200), and (211), respectively. Crystalline iron confirms the presence of metallic Fe as the active phase for the Fenton reaction. Additionally, the dominance of α-Fe suggests that the material is mostly pure iron, with minimal secondary phases. Finally, high crystallinity ensures good electron transfer and stability in the EFT. Inchaurrondo *et al*., reported that slag enriched with magnetite and hematite provided superior performance in Fenton-like oxidation due to its crystalline structure [74].

3.7 *Comparison between IW performance and traditional homogeneous EFT with iron salts*

The reaction kinetics in the electro-Fenton process are influenced by the availability and cycling of Fe^{2+}/Fe^{3+} ions, which act as catalysts in generating hydroxyl radicals ($OH^{\bullet}$). For iron waste systems (EFIW), iron waste provides a gradual release of Fe^{2+} ions into the solution through dissolution, which contributes to continuous $OH^{\bullet}$ generation [75]. However, the dissolution rate is influenced by factors such as pH, particle size, and composition of the waste. In addition to homogeneous reactions, surface reactions occur at the waste material, enabling a combined heterogeneous-homogeneous mechanism that can enhance reaction rates. While in a homogeneous EF system with iron salts (EFIS), soluble iron salts (e.g., $FeSO_4.7H_2O$) provide readily available Fe^{2+} ions, leading to faster reaction kinetics initially. Additionally, Fe^{2+} ions are consumed quickly, and the cycling to Fe^{3+} requires a stable applied potential, which can limit long-term efficiency if not optimized [71].

In terms of efficiency, The MO removal efficiency using iron waste reached 98.82% after 35 minutes, which is comparable to that achieved by Fe^{2+}salts under similar operating conditions. In addition, the presence of impurities in iron waste, such as carbon, may enhance the efficiency by facilitating electron transfer during the reaction. Furthermore, using iron waste avoids the need for synthetic iron salts, reducing costs and environmental impact. Also, the gradual release of Fe^{2+} minimizes the risk of excess Fe^{2+} in treated water, improving compliance with effluent discharge standards [76]. On the other hand, homogeneous EF systems with Fe^{2+} salts typically exhibit higher initial removal rates due to the instantaneous availability of Fe^{2+}ions. However, the excessive use of Fe^{2+} salts can lead to secondary pollution and increased sludge production, which is a drawback compared to the slower iron release in the waste-based system [77], [71].

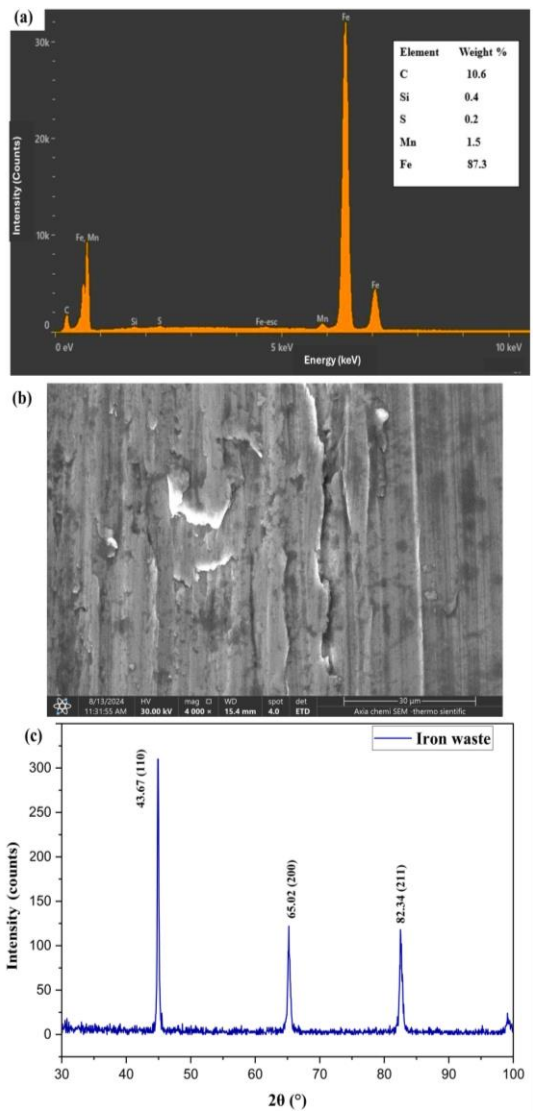

Figure 13: Characterization of IW (a) EDX analysis, (b) SEM image, and XRD pattern.

3.8 *Comparison of earlier studies for MO degradation using Fenton-based advanced oxidation processes (AOPs)*

Table 10 presents a summary of the findings from previous studies on the degradation of MO using AOPs based on the Fenton principle. The comparison highlights key factors like the MO initial concentration [MO_0], the type and dosage of utilized catalysts, the presence or absence of externally added H_2O_2, reaction durations, and the overall efficiency in dye removal, to offer a clear overview of the performance of each method. It could be perceived that the completed removal of 100 mg/L of MO, which was achieved by heterogeneous photo-Fenton needed 60 min of treatment [78] and by using heterogeneous Fenton-like it required 180 min for degrading 92.8% of 15 mg/L of MO [27]. Therefore, EFTs had proven their activity for removing MO at high concentrations with low treatment time compared to photo-Fenton and Fenton processes. Furthermore, our system (EFT with Cf cathode) was superior to the rest of the EFTs mentioned in Table 10, where it achieved more than 98% degradation of MO from a high concentration (100 mg/L) in a time of 35 min. For higher MO concentration, the lower degradation efficiency would be accomplished and the treatment would require a longer time to perform higher removal [78], [60]. Moreover, the current work generated H_2O_2 electrically and also iron salts (Fenton catalyst) could be replaced with iron waste as an economically efficient alternative.

Table 10: Comparison of Fenton-based AOPs performance for MO degrading.

Type of AOPs	$[MO]_o$, mg/L	Catalyst/dose	$[H_2O_2]_o$	Time, min	$\%Re_{MO}$	Ref.
Photo-Fenton	2.5	α-Fe_2O_3 / 30 mg	30 µL	120	76.5	[79]
Heterogeneous photo-Fenton	100	Fe-sand /1.5 g/L	200 mg/L	60	100	[78]
Homogenous electro-Fenton	75	Fe^{2+} / 10^{-4} M	5×10^{-2} M	30	99.37	[60]
Homogenous electro-Fenton	60	Fe^{2+} / 0.232 mM	8.8 mM	60	94.5	[63]
Heterogeneous Fenton-like	15	WO_3 / 2.44 mg/L	0.179 mM/L	180	92.8	[27]
Homogenous electro-Fenton	100	Fe^{2+} / 0.124 mM	-	35	98.68	This work
Heterogeneous electro-Fenton	100	Iron waste	-	35	98.82	This work

Table 11: Comparison of EFT performance for dye removal in terms of EC.

Dye	$[Dye]_o$, mg/L	Electrolysis Time, min	Removal Efficiency (%)	EC, kWh/m^3	Ref.
Diperse Red 1 (DR1)	163.46 [a]	40	90 (in 360 min)	2.4	[80]
Diperse Yellow 3 (DY3)	143.03 [b]	60	90 (in 360 min)	3.6	[80]
Textile wastewater	94 (COD)	30	89	16	[81]
MO	20	15	98	39.4	[82]
Erthrosine B (EB)	100	120	≥90	≥20	[83]
Erthrosine B (EB)	100	30	98.15	0.74	[35]
MO	100	35	98.86	0.7833	This work

As an important notification, the units of some values have been changed for the purpose of harmonizing them with the rest of the values for comparison, where: a: $[DR1]_o$= 0.52 mmol/dm^3, b: $[DY3]_o$= 0.558 mmol/dm^3, and c: EC = 7.87 kWh/kgMO.

3.9 *The energy consumption (EC) comparison with other EFT for dye removal*

Energy consumption (EC) is a critical parameter when evaluating the efficiency of Electrochemical Advanced Oxidation Processes (EAOPs). To highlight the effectiveness of this study, Table 11 summarizes an overview comparison of the EC of this work versus other batch mode EFT reported in the literature for dye removal.

As seen in Table 11, the range of EC was (0.74 to 39.4 kWh/m^3). Clearly, the superiority of the system in this study over the rest of the EF systems is evident, as it removed dye (MO) with high efficiency and minimal EC. Compared to the study conducted by Kacem *et al.*, for removing EB dye by EFT, it can be noted that the EC was slightly more efficient than the system used in this study. The reason is due to the operational conditions used, where a high air flow rate (3 LPM) and a larger mixing speed (500 rpm) were utilized besides using higher electrolyte concentration (0.5 M). All these factors lead to an increase in the dissolved oxygen concentration, thus increasing the electrical generation of H_2O_2, which is an essential factor in the process of $OH^{\bullet}$ generation [62]. Furthermore, increasing the mixing speed improved

the mass transfer of the treated solution and the higher concentration of the electrolyte improved the conductivity of the solution and finally reduced EC and electrolysis time to achieve high removal efficiency [56], [60].

4 Conclusions

The current work studied the influence of various operating parameters such as current density (CD), air flow rate, and the concentration of catalyst [Fe^{2+}] on the degradation of methyl orange (MO) through Electro-Fenton technology (EFT) using anode and cathode of porous graphite (PG) and copper foam (Cf) respectively. Optimization method achieved using Box-Behnken (BB) approach. The best removal efficiency (%Re_{MO}) was 98.86% with energy consumption (EC) of 7.88 kWh/kg MO, which was performed at optimal conditions (CD = 5.22 mA/cm^2, air flow = 0.3 LPM, and [Fe^{2+}] = 0.124 mM). Furthermore, the present study revealed that the use of Cf as a working electrode in EFT was very successful as it achieved high degradation of MO in a relatively short time (35 min) with the possibility of reusing the cathode for 3 consecutive cycles with no need for regeneration process and at acceptable concentrations of copper leaching from Cf cathode. To further mitigate leaching beyond three cycles and enhance cathode stability, some measures can be followed such as rinsing the cathode with diluted acidic solutions or ultrasonic cleaning to remove fouling or applying thin oxide layers on the copper foam to prevent corrosion or integrating copper foam with carbon nanotubes or metal oxides to enhance durability. On the other hand, the outcomes proved that EFT was the dominant process for the removal of MO, as %Re_{MO} was 98.6% while anodic oxidation (AO) attained 76.7% at the same conditions. The utilization of iron waste (heterogeneous EFT) instead of iron salts (homogenous EFT) as an economical source of Fenton catalyst revealed great %Re_{MO} (98.82%) besides, the heterogeneous catalyst (IW) demonstrated excellent reusability, showing only minor iron leaching, and preserving its stability throughout 4 successive runs. However, this system shows great potential as an ideal choice for developing EFTs that run continuously. On the other hand, while the system performed effectively under controlled conditions, the real wastewater may present challenges due to its variable pH, ionic composition, and organic load. Further investigations with real wastewater are necessary to validate the system's scalability and adaptability. Moreover, future research should focus on elucidating the MO degradation mechanism and reaction pathways to further enhance the system's efficiency and applicability.

Author Contributions

Z. M. H.: investigation, methodology, writing an original draft, research design, data analysis; R. H. S.: conceptualization, data curation, writing—reviewing and editing, research design, data analysis, project administration. Both authors have read and agreed to the published version of the manuscript.

Conflicts of Interest

The authors declare no conflict of interest.

References

[1] S. Yadav and S. Kamsonlian, "Progress on the development of techniques to remove contaminants from wastewater: A review," *Applied Science and Engineering Progress*, vol. 16, no. 3, Feb. 2023, Art. no. 6729, doi: 10.14416/j.asep.2023.02.001.

[2] C. O. Okafor, U. I. Ude, F. N. Okoh, and B. O. Eromonsele, "Safe drinking water: The need and challenges in developing countries," in *Water Quality-New Perspectives*. London, UK: IntechOpen, 2024, doi: 10.5772/intechopen.108497.

[3] UNESCO. "The United Nations World Water Development Report." unesco.org. https://www.unesco.org/reports/wwdr/2021/en (accessed Jan. 13, 2025).

[4] F. and A. O. of the U. Nation. "The State of Food and Agriculture 2020: Overcoming Water Challenges in Agriculture." fao.org. http://www.fao.org/state-of-food-agriculture/2020 (accessed Jan. 13, 2025).

[5] R. Al-Tohamy, S. S. Ali, F. Li, K. M. Okasha, Y. A.-G. Mahmoud, T. Alsamahy, H. Jiao, Y. Fu, and J. Sun, "A critical review on the treatment of dye-containing wastewater: Ecotoxicological and health concerns of textile dyes and possible remediation approaches for environmental safety," *Ecotoxicology and Environmental Safety*, vol. 231, Feb. 2022, Art. no. 113160, doi: 10.1016/j.ecoenv.2021.113160.

[6] M. M. El-Sadaawy and N. S. Agib, "Removal of

textile dyes by ecofriendly aquatic plants from wastewater: A review on plants species, mechanisms, and perspectives," *Blue Economy*, vol. 2, no. 2, Jul. 2024, doi: 10.57241/2805-2994.1023.

[7] P. Kiattisaksiri, N. Petmark, and T. Ratpukdi, "Combination of coagulation and VUV+H_2O_2 for the treatment of color and organic matter in treated effluent wastewater from a sugar factory," *Applied Science and Engineering Progress*, vol. 16, no. 4, 2022, Art. no. 6192, doi: 10.14416/j.asep.2022.08.002.

[8] H. J. Nsaif, N. S. Majeed, and R. H. Salman, "Preparation of nano SnO_2-Sb_2O_3 composite electrode by cathodic deposition for the elimination of phenol by Sonoelectrochemical oxidation," *Polish Journal of Chemical Technology*, vol. 26, no. 3, pp. 21–28, Sep. 2024, doi: 10.2478/pjct-2024-0026.

[9] A. B. D. Nandiyanto, S. N. Hofifah, H. T. Inayah, I. F. Yani, S. R. Putri, S. S. Apriliani, S. Anggraeni, D. Usdiyana and A. Rahmat, "Adsorption isotherm of carbon microparticles prepared from pumpkin (*cucurbita maxima*) seeds for dye removal," *Iraqi Journal of Science*, vol. 62, no. 5, pp. 1404–1414, May 2021, doi: 10.24996/ijs.2021.62.5.2.

[10] M. Abewaa, E. Adino, and A. Mengistu, "Preparation of Rumex abyssinicus based biosorbent for the removal of methyl orange from aqueous solution," *Heliyon*, vol. 9, no. 12, Dec. 2023, Art. no. e22447, doi: 10.1016/j.heliyon.2023.e22447.

[11] S. Yadav, K. S. Tiwari, C. Gupta, M. K. Tiwari, A. Khan, and S. P. Sonkar, "A brief review on natural dyes, pigments: Recent advances and future perspectives," *Results in Chemistry*, vol. 5, Jan. 2023, Art. no. 100733, doi: 10.1016/j.rechem.2022.100733.

[12] W. W. Leow, A. Duke, S. K. E. Ab Rahim, Q. H. Ng, P. Y. Hoo, A. M. Nasib, M. Q. Z. A. Suffin and N. S. Abdullah, "Facile synthesis of hybrid-polyoxometalates nanocomposite for degradation of cationic and anionic dyes in water treatment," *Applied Science and Engineering Progress*, vol. 18, no. 1, Jul. 2024, Art. no. 7485, doi: 10.14416/j.asep.2024.07.014.

[13] A. Kumar, U. Dixit, K. Singh, S. Prakash Gupta, and M. S. Jamal Beg, "Structure and properties of dyes and pigments," in *Dyes and Pigments-Novel Applications and Waste Treatment*. London, UK: IntechOpen, 2021, doi: 10.5772/intechopen.97104.

[14] A. G. Saleem and S. M. Al-Jubouri, "Efficient separation of organic dyes using polyvinylidene fluoride/polyethylene glycol-tin oxide (PVDF/PEG-SnO_2) nanoparticles ultrafiltration membrane," *Applied Science and Engineering Progress*, vol. 17, no. 4, 2024, Art. no. 7523, doi: 10.14416/j.asep.2024.08.001.

[15] M. A. Mohammed, W. O. Noori, and H. A. Sabbar, "Application of emulsion liquid membrane process for cationic dye extraction," *Iraqi Journal of Chemical and Petroleum Engineering*, vol. 21, no. 3, pp. 39–44, Sep. 2020, doi: 10.31699/IJCPE.2020.3.5.

[16] R. H. Salman, E. M. Khudhair, K. M. Abed, and A. S. Abbas, "Removal of E133 brilliant blue dye from artificial wastewater by electrocoagulation using cans waste as electrodes," *Environmental Progress & Sustainable Energy*, vol. 43, no. 2, Mar. 2024, Art. no. e14292, doi: 10.1002/ep.14292.

[17] N. A. Mohammed, A. I. Alwared, and M. S. Salman, "Photocatalytic degradation of reactive yellow dye in wastewater using H_2O_2/TiO_2/UV technique," *Iraqi Journal of Chemical and Petroleum Engineering*, vol. 21, no. 1, pp. 15–21, Mar. 2020, doi: 10.31699/IJCPE.2020.1.3.

[18] S. K. A. Barno, H. J. Mohamed, S. M. Saeed, M. J. Al-Ani, and A. S. Abbas, "Prepared 13X zeolite as a promising adsorbent for the removal of brilliant blue dye from wastewater," *Iraqi Journal of Chemical and Petroleum Engineering*, vol. 22, no. 2, pp. 1–6, Jun. 2021, doi: 10.31699/IJCPE.2021.2.1.

[19] Z. M. Hameed and R. H. Salman, "Elimination of methyl orange dye with three dimensional electro-fenton and sono-electro-fenton systems utilizing copper foam and activated carbon," *Ecological Engineering & Environmental Technology*, vol. 25, no. 10, pp. 44–59, Oct. 2024, doi: 10.12912/27197050/191199.

[20] T. M. Tamer, R. Abbas, W. A. Sadik, A. M. Omer, M. M. Abd-Ellatif, and M. S. Mohy-Eldin, "Development of novel amino-ethyl chitosan hydrogel for the removal of methyl orange azo dye model," *Scientific Reports*, vol. 14, no. 1, p. 1284, Jan. 2024, doi: 10.1038/s41598-024-51538-1.

[21] M. A. B. Aissa, M. Khairy, M. E. Khalifa, E. A. Abdelrahman, N. Raza, E. M. Masoud, and A. Modwi, "Facile synthesis of TiO2@ZnO nanoparticles for enhanced removal of methyl orange and indigo carmine dyes: Adsorption,

kinetics," *Heliyon*, vol. 10, no. 10, p. e31351, May 2024, doi: 10.1016/j.heliyon.2024.e31351.

[22] M. A. Mohammed, I. S. Al-Bayati, A. A. Alobaidy, B. I. Waisi, and N. Majeed, "Investigation the efficiency of emulsion liquid membrane process for malachite green dye separation from water," *Desalination and Water Treatment*, vol. 307, pp. 190–195, Nov. 2023, doi: 10.5004/dwt.2023.29903.

[23] I. A. Abed and B. I. Waisi, "Preparation and characterization of PES flat sheet membrane embedded with PEG for dye filtration application," *Iraqi Journal of Applied Physics*, vol. 20, no. 2, pp. 179–186, 2024.

[24] A. E. Alprol, M. Khedawy, M. Ashour, and W. M. Thabet, "*Arthrospira platensis* nanoparticle-based approach for efficient removal of methyl orange dye from aqueous solutions: isotherm, kinetic, and thermodynamic analysis," *Biomass Conversion and Biorefinery*, vol. 14, pp. 30279–30296, Oct. 2023, doi: 10.1007/s13399-023-04844-z.

[25] S. H. Abbas, Y. M. Younis, K. H. Rashid, and A. A. Khadom, "Removal of methyl orange dye from simulated wastewater by electrocoagulation technique using Taguchi method: kinetics and optimization approaches," *Reaction Kinetics, Mechanisms and Catalysis*, vol. 135, no. 5, pp. 2663–2679, Oct. 2022, doi: 10.1007/s11144-022-02269-9.

[26] N. A. A. Mohammed, A. I. Alwared, and M. S. Salman, "Decolorization of reactive yellow dye by advanced oxidation using continuous reactors," *Iraqi Journal of Chemical and Petroleum Engineering*, vol. 21, no. 2, pp. 1–6, Jun. 2020, doi: 10.31699/IJCPE.2020.2.1.

[27] N. S. Eroi, A. S. Ello, D. Diabaté, and K. R. Koffi, "Kinetic study of the removal of methyl orange dye by coupling WO_3/H_2O_2," *Journal of Chemistry*, vol. 2022, pp. 1–8, Sep. 2022, doi: 10.1155/2022/8633545.

[28] A. S. Adday and S. M. Al-Jubouri, "Photocatalytic oxidative removal of the organic pollutant from wastewater using recyclable Ag_2O@CRA heterojunction photocatalyst," *Case Studies in Chemical and Environmental Engineering*, vol. 10, Dec. 2024, Art. no. 100852, doi: 10.1016/j.cscee.2024.100852.

[29] F. E. Titchou, H. Zazou, H. Afanga, J. E. Gaayda, R. A. Akbour, P. V. Nidheesh, and M. Hamdani, "Removal of organic pollutants from wastewater by advanced oxidation processes and its combination with membrane processes," *Chemical Engineering and Processing - Process Intensification*, vol. 169, Dec. 2021, Art. no. 108631, doi: 10.1016/j.cep.2021.108631.

[30] G. V. Serban, V. I. Iancu, C. Dinu, A. Tenea, N. Vasilache, I. Cristea, M. Niculescu, I. Ionescu, and F. L. Chiriac, "Removal efficiency and adsorption kinetics of methyl orange from wastewater by commercial activated carbon," *Sustainability*, vol. 15, no. 17, Art. no. 12939, Aug. 2023, doi: 10.3390/su151712939.

[31] D. Ma, H. Yi, C. Lai, X. Liu, X. Huo, Z. An, L. Li, Y. Fu, B. Li, M. Zhang, L. Qin, S. Liu, and L. Yang, "Critical review of advanced oxidation processes in organic wastewater treatment," *Chemosphere*, vol. 275, Jul. 2021, Art. no. 130104, doi: 10.1016/j.chemosphere.2021.130104.

[32] L. Song, C. Liu, L. Liang, Y. Ma, X. Wang, J. Ma, Z. Li, and S. Yang, "Fabrication of PbO2/PVDF/CC composite and employment for the removal of methyl orange," *Polymers (Basel)*, vol. 15, no. 6, p. 1462, Mar. 2023, doi: 10.3390/polym15061462.

[33] C. F. Carolin, P. S. Kumar, and G. J. Joshiba, "Sustainable approach to decolourize methyl orange dye from aqueous solution using novel bacterial strain and its metabolites characterization," *Clean Technologies and Environmental Policy*, vol. 23, no. 1, pp. 173–181, Jan. 2021, doi: 10.1007/s10098-020-01934-8.

[34] A. Latha, R. Ganesan, A. V. S. L. Sai Bharadwaj, and P. Barmavatu, "An experimental investigation of textile dyeing wastewater using modified electro Fenton process with optimization by response surface methodology," *Environmental Quality Management*, vol. 33, no. 3, pp. 421–432, Mar. 2024, doi: 10.1002/tqem.22135.

[35] S. Ben Kacem, D. Clematis, S. C. Elaoud, and M. Panizza, "Response surface methodology for low-energy consumption electro-Fenton process for xanthene dye electrochemical degradation," *Journal of Applied Electrochemistry*, vol. 54, no. 9, pp. 2095–2110, Sep. 2024, doi: 10.1007/s10800-024-02087-y.

[36] H. Olvera-Vargas, N. Gore-Datar, O. Garcia-Rodriguez, S. Mutnuri, and O. Lefebvre, "Electro-Fenton treatment of real pharmaceutical wastewater paired with a BDD anode: Reaction mechanisms and respective contribution of homogeneous and hetrogeneous OH," *Chemical*

Engineering Journal, vol. 404, Jan. 2021, Art. no. 126524, doi: 10.1016/j.cej.2020.126524.

[37] G. D. Değermenci and N. Değermenci, "Electrochemical hydrogen peroxide generation and removal of moxifloxacin by electro-fenton process," *Black Sea Journal of Engineering and Science*, vol. 7, no. 3, pp. 539–546, May 2024, doi: 10.34248/bsengineering.1461577.

[38] A. Limper, M. Mohseni, R. Keller, J. Linkhorst, J. Klankermayer, and M. Wessling, "An electrode with two-level porosity for electro-Fenton: Carbon nanofiber-functionalized macroporous nickel foam," *Advanced Sustainable Systems*, vol. 7, no. 3, Mar. 2023, doi: 10.1002/adsu.202200408.

[39] B. Ma, W. Lv, J. Li, C. Yang, Q. Tang, and D. Wang, "Promotion removal of aniline with electro-Fenton processes utilizing carbon nanotube 3D morphology modification of an Ag-loaded copper foam cathode," *Journal of Water Process Engineering*, vol. 43, Oct. 2021, Art. no. 102295, doi: 10.1016/j.jwpe.2021.102295.

[40] J. Li, D. Song, K. Du, Z. Wang, and C. Zhao, "Performance of graphite felt as a cathode and anode in the electro-Fenton process," *Royal Society of Chemistry Advances*, vol. 9, no. 66, pp. 38345–38354, 2019, doi: 10.1039/C9RA07525A.

[41] M. Vainoris, A. Nicolenco, N. Tsyntsaru, E. Podlaha-Murphy, F. Alcaide, and H. Cesiulis, "Electrodeposited Fe on Cu foam as advanced fenton reagent for catalytic mineralization of methyl orange," *Frontiers Chemsitry*, vol. 10, Sep. 2022, doi: 10.3389/fchem.2022.977980.

[42] E. Bocos, O. Iglesias, M. Pazos, and M. Ángeles Sanromán, "Nickel foam a suitable alternative to increase the generation of Fenton's reagents," *Process Safety and Environmental Protection*, vol. 101, pp. 34–44, May 2016, doi: 10.1016/j.psep.2015.04.011.

[43] Y. Zheng, S. Qiu, F. Deng, Y. Zhu, G. Li, and F. Ma, "Three-dimensional electro-Fenton system with iron foam as particle electrode for folic acid wastewater pretreatment," *Separation and Purification Technology*, vol. 224, pp. 463–474, Oct. 2019, doi: 10.1016/j.seppur.2019.05.054.

[44] G. Li, S. Qiu, Y. Zhu, F. Deng, and F. Ma, "Utilization of response surface modeling to optimize hydrogen peroxide and hydroxyl radicals generation by electro-Fenton with copper-foam as cathode," *Chinese Journal of Environmental Engineering*, vol. 12, no. 1, pp. 93–101, Jan. 2018, doi: 10.12030/j.cjee.201706051.

[45] T. Qian, S. Juan, R. Xiaolei, Y. Chunwei and W. Dong, "Comparative study on the electro-Fenton-like oxidation of p-nitrophenol with nickel and copper foam cathodes," *Chemical Industry and Engineering Progress*, vol. 36, no. 7, pp. 2653–2659, 2017, doi: 10.16085/j.issn.1000-6613.2016-2070.

[46] R. N. Abbas, "Advanced electro-oxidation of phenol in refinery wastewater using graphite and carbon fiber electrodes modified with PbO_2 and graphene," Ph.D. dissertation, Depattment of Chemical Engineering, Baghdad University, Baghdad, Iraq, 2022.

[47] P. Brosler, A. V. Girão, R. F. Silva, J. Tedim, and F. J. Oliveira, "Electrochemical advanced oxidation processes using diamond technology: A critical review," *Environments*, vol. 10, no. 2, p. 15, Jan. 2023, doi: 10.3390/environments 10020015.

[48] P. V. Nidheesh, H. Olvera-Vargas, N. Oturan, and M. A. Oturan, "Heterogeneous electro-Fenton process: Principles and applications," in *Electro-Fenton Process*, vol. 61, M. Zhou, M. A. Oturan, and I. Sirés, Eds. Singapore: Springer, pp. 85–110, 2017. doi: 10.1007/698_2017_72.

[49] H. H. Thwaini and R. H. Salman, "Phenol removal by electro-Fenton process using a 3D electrode with iron foam as particles and carbon fibre modified with graphene," *Journal of Electrochemical Science and Engineering*, vol.13, no. 3, Jun. 2023, doi: 10.5599/jese.1806.

[50] A. Shokri, B. Nasernejad, and M. Sanavi Fard, "Challenges and future roadmaps in heterogeneous electro-Fenton process for wastewater treatment," *Water, Air, and Soil Pollution*, vol. 234, no. 3, p. 153, Mar. 2023, doi: 10.1007/s11270-023-06139-5.

[51] P. Fedorko, A. Pribulová, J. Petrík, P. Blaško, and P. Futáš, "The impact of iron casting in cupola furnaces on the environment," in *MM 2023*, Basel, Switzerland: MDPI, Feb. 2024, vol. 64, p. 8, doi: 10.3390/engproc2024064008.

[52] M. Priyadarshini, A. Ahmad, and M. M. Ghangrekar, "Efficient upcycling of iron scrap and waste polyethylene terephthalate plastic into Fe_3O_4@C incorporated MIL-53(Fe) as a novel electro-Fenton catalyst for the degradation of salicylic acid," *Environmental Pollution*, vol. 322, Apr. 2023, Art. no. 121242, doi: 10.1016/ j.envpol.2023.121242.

[53] A. Saber, S. Mortazavian, D. E. James, and H. Hasheminejad, "Optimization of collaborative

photo-Fenton oxidation and coagulation for the treatment of petroleum refinery wastewater with scrap iron," *Water, Air, and Soil Pollution*, vol. 228, no. 8, p. 312, Aug. 2017, doi: 10.1007/s11270-017-3494-2.

[54] N. Nippatla and L. Philip, "Electrochemical process employing scrap metal waste as electrodes for dye removal," *Journal of Environmental Management*, vol. 273, Nov. 2020, doi: 10.1016/j.jenvman.2020.111039.

[55] C. Xia and X. Shen, "Analysis of factors influencing on electro-Fenton and research on combination technology (II): A review," *Environmental Science and Pollution Research*, vol. 31, no. 34, pp. 46910–46948, Jul. 2024, doi: 10.1007/s11356-024-34159-z.

[56] H. He and Z. Zhou, "Electro-Fenton process for water and wastewater treatment," *Critical Reviews In Environmental Science and Technology*, vol. 47, no. 21, pp. 2100–2131, Nov. 2017, doi: 10.1080/10643389.2017.1405673.

[57] M. I. Syauqi, A. T. Cahyani, Y. M. T. A. Putri, and P. K. Jiwanti, "Electroreduction of carbon dioxide (CO_2) with flow cell system using tin-modified copper foam electrode," *Environmental and Materials*, vol. 1, no. 2, Dec. 2023, doi: 10.61511/eam.v1i2.2023.363.

[58] M. M. Jiad and A. H. Abbar, "Efficient wastewater treatment in petroleum refineries: Hybrid electro-fenton and photocatalysis (UV/ZnO) process," *Chemical Engineering Research and Design*, vol. 200, pp. 431–444, Dec. 2023, doi: 10.1016/j.cherd.2023.10.050.

[59] M. M. Jiad and A. H. Abbar, "Treatment of petroleum refinery wastewater by electrofenton process using a low cost porous graphite air-diffusion cathode with a novel design," *Chemical Engineering Research and Design*, vol. 193, pp. 207–221, May 2023, doi: 10.1016/j.cherd.2023.03.021.

[60] Z. Benredjem, K. Barbari, I. Chaabna , S. Saaidia, A. Djemel, R. Delimi, S. Douas and K. Bakhouche, "Comparative investigation on the removal of methyl orange from aqueous solution using three different advanced oxidation processes," *International Journal of Chemical Reactor Engineering*, vol. 19, no. 6, pp. 597–604, Jun. 2021, doi: 10.1515/ijcre-2020-0243.

[61] H. H. Thawini, R. H. Salman, and W. S. Abdul-Majeed, "Performance of electro-Fenton process for phenol degradation using nickel foam as a cathode," *Iraqi Journal of Chemical and Petroleum Engineering*, vol. 24, no. 3, pp. 13–25, 2023, doi: 10.31699/ijcpe.2023.3.2.

[62] S. Midassi, A. Bedoui, and N. Bensalah, "Efficient degradation of chloroquine drug by electro-Fenton oxidation: Effects of operating conditions and degradation mechanism," *Chemosphere*, vol. 260, p. 127558, Dec. 2020, doi: 10.1016/j.chemosphere.2020.127558.

[63] A. Adachi, F. E. Ouadrhiri, M. Kara, I. E. Manssouri, A. Assouguem, M. H. Almutairi, R. Bayram, H. R. H. Mohamed, I. Peluso, N. Eloutassi, and A. Lahkimi, "Decolorization and degradation of methyl orange azo dye in aqueous solution by the electro-Fenton process: application of optimization," *Catalysts*, vol. 12, no. 6, p. 665, Jun. 2022, doi: 10.3390/catal12060665.

[64] Y. Zou, H. Qi, and Z. Sun, "In-situ catalytic degradation of sulfamethoxazole with efficient CuCo–O@CNTs/NF cathode in a neutral electro-Fenton-like system," *Chemosphere*, vol. 296, Jun. 2022, Art. no. 134072, doi: 10.1016/j.chemosphere.2022.134072.

[65] S. Zhong, Z. Zhu, P. Zhou, L. Shi, X. Duan, B. Lai, and S. Wang, "FeOCl nanoparticles loaded on to oxygen-enriched carbon nanotubes and nickel-foam-based cathodes for the electro-Fenton degradation of pollutants," *American Chemical Society Applied Nano Materials*, vol. 5, no. 9, pp. 12095–12106, Sep. 2022, doi: 10.1021/acsanm.2c01413.

[66] National Research Council (US) Committee on Copper in Drinking Water, *Copper in Drinking Water*. Washington DC: National Academies Press, 2000.

[67] S. M. Al-Jubouri, R. H. Salman, E. M. Khudhair, A. S. Abbas, A. F. Al-Alawy, S. Y. Khudhair, M. H. Salih, H. A. Hassan and A. Alfutimie, "Multicomponent equilibrium isotherms and kinetics study of heavy metals removal from aqueous solutions using electrocoagulation combined with mordenite zeolite and ultrasonication," *Applied Science and Engineering Progress*, vol. 18, no. 1, 2025, Art. no. 7484 doi: 10.14416/j.asep.2024.07.011.

[68] S. Sultana, M. R. Choudhury, A. R. Bakr, N. Anwar, and M. S. Rahaman, "Effectiveness of electro-oxidation and electro-Fenton processes in removal of organic matter from high-strength brewery wastewater," *Journal of Applied*

Electrochemistry, vol. 48, no. 5, pp. 519–528, May 2018, doi: 10.1007/s10800-018-1185-3.

[69] C. Martínez-Sánchez, I. Robles, and L. A. Godínez, "Review of recent developments in electrochemical advanced oxidation processes: application to remove dyes, pharmaceuticals, and pesticides," *International journal of Environmental Science and Technology*, vol. 19, no. 12, pp. 12611–12678, Dec. 2022, doi: 10.1007/s13762-021-03762-9.

[70] X. Wang, J. Zhao, C. Song, X. Shi, and H. Du, "An eco-friendly iron cathode electro-Fenton system coupled with a pH-regulation electrolysis cell for p-nitrophenol degradation," *Frontiers Chemsitry*, vol. 9, Jan. 2022, doi: 10.3389/fchem.2021.837761.

[71] Z. Heidari, R. Pelalak, R. Alizadeh, N. Oturan, S. Shirazian, and M. A. Oturan, "Application of mineral iron-based natural catalysts in electro-Fenton process: A comparative study," *Catalysts*, vol. 11, no. 1, p. 57, Jan. 2021, doi: 10.3390/catal11010057.

[72] N. Rattanachueskul, P. Onsri, W. Watcharin, A. Makarasen, S. Techasakul, D. Dechtrirat and L. Chuenchom, "Waste para-rubber wood ash and iron scrap for the sustainable preparation of magnetic Fenton catalyst for efficient degradation of tetracycline," *Arabian Journal of Chemistry*, vol. 17, no. 6, Jun. 2024, Art. no. 105791, doi: 10.1016/j.arabjc.2024.105791.

[73] S. M. H. Kazmi, J. Du, X. Zhao, M. Faheem, A. Hassan, M. Yousuf, H. Zheng, and C. Yi, "Transforming waste to purity: 3D electro-Fenton process boosted with pistachio shell-derived iron-biochar electrode for methyl violet 2B dye catalytic removal," *Desalination and Water Treatment*, vol. 320, Oct. 2024, Art. no. 100845, doi: 10.1016/j.dwt.2024.100845.

[74] N. S. Inchaurrondo, F. Bocero, C. P. Ramos, T. Freije, and L. A. Fasce, "Enhanced mineralization of bisphenol A by electric arc furnace slag: Fenton-like oxidation," *Applied Catalysis O: Open*, vol. 193, Aug. 2024, Art. no. 206971, doi: 10.1016/j.apcato.2024.206971.

[75] G. Khajouei, S. Mortazavian, A. Saber, N. Z. Meymian, and H. Hasheminejad, "Treatment of composting leachate using electro-Fenton process with scrap iron plates as electrodes," *International journal of Environmental Science and Technology*, vol. 16, no. 8, pp. 4133–4142, Aug. 2019, doi: 10.1007/s13762-018-2057-4.

[76] S. Ammar, M. A. Oturan, L. Labiadh, A. Guersalli, R. Abdelhedi, N. Outrun, and E. Brillas, "Degradation of tyrosol by a novel electro-Fenton process using pyrite as heterogeneous source of iron catalyst," *Water Research*, vol. 74, pp. 77–87, May 2015, doi: 10.1016/j.watres.2015.02.006.

[77] M. A. Oturan and J.-J. Aaron, "Advanced oxidation processes in water/wastewater treatment: Principles and applications. A review," *Critical Reviews in Environmental Science and Technology*, vol. 44, no. 23, pp. 2577–2641, Dec. 2014, doi: 10.1080/10643389.2013.829765.

[78] A. Omri, W. Hamza, and M. Benzina, "Photo-Fenton oxidation and mineralization of methyl orange using Fe-sand as effective heterogeneous catalyst," *Journal of Photochemistry and Photobiology A: Chemistry*, vol. 393, Apr. 2020, Art. no. 112444, doi: 10.1016/j.jphotochem.2020.112444.

[79] A. M. G. Domacena, C. L. E. Aquino, and M. D. L. Balela, "Photo-Fenton degradation of methyl orange using hematite (α-Fe_2O_3) of various morphologies," *Materials Today: Proceedings*, vol. 22, pp. 248–254, Feb. 2020, doi: 10.1016/j.matpr.2019.08.095.

[80] R. Salazar, S. Garcia-Segura, M. S. Ureta-Zañartu, and E. Brillas, "Degradation of disperse azo dyes from waters by solar photoelectro-Fenton," *Electrochimica Acta*, vol. 56, no. 18, pp. 6371–6379, Jul. 2011, doi: 10.1016/j.electacta.2011.05.021.

[81] A. Kuleyin, A. Gök, and F. Akbal, "Treatment of textile industry wastewater by electro-Fenton process using graphite electrodes in batch and continuous mode," *Journal of Environmental Chemical Engineering*, vol. 9, no. 1, p. 104782, Feb. 2021, doi: 10.1016/j.jece.2020.104782.

[82] A. S. Naje, I. S. Samaka, H. M. Zwain, and M. A. Ajeel, "Photovoltaic cell electro-Fenton oxidation process for treatment of organic content in methyl orange wastewater," *Journal of Sustainability Science and Management*, vol. 16, no. 4, pp. 53–63, Jun. 2021, doi: 10.46754/jssm.2021.06.005.

[83] D. Clematis and M. Panizza, "Electro-Fenton, solar photoelectro-Fenton and UVA photoelectro-Fenton: Degradation of erythrosine B dye solution," *Chemosphere*, vol. 270, May 2021, Art. no. 129480, doi: 10.1016/j.chemosphere.2020.129480.